Hydrodynamics of Gas-Liquid Cocurrent Upflow in Oscillating Packed Beds for Offshore Marine Applications

Originally published:

December 2016

Chemical Engineering Science 170(2017)12, 583-596

DOI: https://doi.org/10.1016/j.ces.2016.12.056

Hydrodynamics of Gas-Liquid Cocurrent Upflow in Oscillating Packed Beds for Offshore Marine Applications

Amir Motamed Dashliborun,[a] Faïçal Larachi,[a]* Markus Schubert[b]

[a] Department of Chemical Engineering, Laval University, Québec, QC, Canada G1V 0A6

[b]Helmholtz-Zentrum Dresden-Rossendorf, Bautzner Landstraße 400, 01328 Dresden, Germany
*Corresponding authors: Faical.Larachi@gch.ulaval.ca (F. Larachi)

Abstract In this study, the hydrodynamic behavior of inclined stationary and oscillating packed beds with gas-liquid cocurrent upflow mode of operation was investigated. Comprehensive hydrodynamic experiments were carried out using embedded low-intrusive Wire-Mesh Sensors (WMSs) and a hexapod ship motion simulator in order to properly understand the effect of column inclination and movements on gas-liquid flow distribution in the bed cross-section, overall pressure drop, liquid saturation, and pulsing flow inception. Furthermore, liquid residence time and Péclet number estimated by a stimulus-response technique and a macro-mixing model were presented and discussed with respect to the prevailing flow regimes. The results revealed that the column deviation from the vertical posture and tilting motions significantly alter the hydrodynamics prevailing in the packed bed operating in a concurrent upflow mode. Development of gas-liquid disengagement zones, oscillations in the pressure drop and uniformity factor time series, departure from liquid plug flow character, and delay in the inception of pulsing flow regime were observed as a result of bed inclination and oscillations.

Keywords Cocurrent upflow packed bed; oscillation; wire mesh sensor; hexapod motion simulator; maldistribution; hydrodynamics

1. Introduction

Gas-liquid cocurrent upflow packed beds are commonly used as multiphase contactors and reactors in continuous processes involving chemical reactions which require good contacting between gas, liquid, and solid phases (Duduković et al., 2002; Hofmann, 1983). Wastewater treatment, hydrogenation, oxidation, alkylation, and amination of alcohols are among the processes that have long been carried out in this type of reactors due to low operating costs and simplicity in construction. Furthermore, good inter-phase heat and mass transfers, large liquid residence times, and high interfacial area can be achieved in cocurrent upflow packed bed reactors (Collins et al., 2016).

A random arrangement of solid particles generates a complex network of throats and pores inside the bed resulting in different patterns of the concurrent flow of gas and liquid phases (Ranade et al., 2011). Depending on the packing types, fluids velocities, and physio-chemical properties of gas and liquid phases, three main hydrodynamic regimes, namely, bubbly flow, pulse flow, and spray flow have been reported for cocurrent upflow packed beds (Moreira and Freire, 2003; Murugesan and Sivakumar, 2002; Raghavendra Rao et al., 2011; Varma et al., 1997). In the bubbly flow regime, a discontinuous gas phase in the form of bubbles moves upward within a continuous liquid phase. The pulse flow regime is recognizable from the intermittent liquid-rich and gas-rich pulses traveling through the bed. Spray flow regime occurs at high gas and low liquid flow rates when the majority of liquid is entrained by a continuous gas phase in the form of droplets.

The hydrodynamic complexity of cocurrent upflow packed beds, on the one hand, and the importance of reliable design and scale-up to industrial scale, on the other hand, have attracted numerous researchers to work in the field of cocurrent upflow packed bed reactors. While some

studies have focused on experimental methods to specify the hydrodynamic characteristics such as liquid and gas holdups, bubble properties, pressure drop, flow regime, back mixing, and heat and mas transfer (Collins et al., 2016; Khadilkar et al., 1996; Larachi et al., 1991; Leveque et al., 2016; Vejražka et al., 2010), others ought to develop mathematical models to estimate those hydrodynamic parameters (Attou and Ferschneider, 1999; Jo and Revankar, 2011; Salgi and Balakotaiah, 2014). Most recently, Collins et al. (2016) investigated gas phase dynamics within a packed bed of spherical non-porous particles with cocurrent upflow mode of operation using magnetic resonance imaging techniques. The experimental results revealed that the gas holdup increases with gas flow rate whereas an increase in packing size and liquid flow rate decreases it. Moreover, static gas holdup was found to increase appreciably with decreasing packing size. Leveque et al. (2016) applied stainless steel open-solid foams with different pore densities instead of solid particles as a packing in the cocurrent upflow packed bed. Pressure drop, liquid mean residence time, and axial Péclet number were determined as the main hydrodynamic parameters. They found that the liquid superficial velocity and foam pore density are the most influential parameters on the hydrodynamics of cocurrent upflow packed beds. The existence of bubbly and pulse flow regimes were also recognized from pressure drop measurements.

Currently, oil and gas extraction and processing industries in deeper water and remote offshore areas have led the petroleum industry to extend the functionality of packed beds for applications on floating platforms such as FPSO (floating production storage and offloading) and FLNG (floating liquefied natural gas) (Kim et al., 2014a; Kim et al., 2014b; Shimamura, 2002). In these systems, a large number of processing units including extraction, production, and storage operations are integrated on the same floating platform to ensure economic viability and monetization of stranded hydrocarbon sources (El-Reedy, 2012; Gu and Ju, 2008; Shimamura,

2002; Subrata and Cliakrabarti, 2005). Nevertheless, complex sea states pose considerable technical challenges to operations of onboard packed bed reactors and separators which may ultimately hamper meeting product specification. Ship oscillations and tilts triggered by marine swells impact the hydrodynamics of packed bed reactors and thus their performances. This means that the hydrodynamic features which are relevant to the marine context cannot be directly transposed on a one-to-one basis from ground installations and thus more insights are required for floating reactors. More specifically, experimental and theoretical studies concerning the effect of floating vessel motions on the hydrodynamic behavior of packed bed reactors onboard are of significance.

In recent years, several researchers investigated the hydrodynamics prevailing inside *stationary* tilted packed beds viewed as limiting column postures on ships. Schubert et al. (2010a) and Atta et al. (2010) experimentally and theoretically showed that the bed deviation from the vertical position causes partial gas-liquid segregation in packed beds with gas-liquid descending flows, which in turn diminishes two-phase pressure drop and liquid coverage area. Conversely, Bouteldja et al. (2013) studied the effect of column inclination on the hydrodynamic behavior of packed beds with concurrent gas-liquid upflow mode of operation. Gas-liquid disengagement was found to evolve by incrementing inclination angle as in inclined trickle beds and a gradual transition from bubbly flow to segregated/bubbly flow regimes took place. An increase in the cross-sectionally averaged liquid saturation and a decrease in pressure drop were also observed as a result of inclining the vessel. Besides, examination of the hydrodynamics of gas-liquid countercurrent packed beds under column obliquity divulged a noticeable reduction of the overall pressure drop and liquid saturation, in addition to a delay to the onset of flooding and an aggravation of phase maldistribution (Wongkia et al., 2015).

Furthermore, packed beds operated with gas-liquid cocurrent downflow in stationary tilted and oscillating configurations were experimentally investigated by Assima et al. (2015b) and Motamed Dashliborun and Larachi (2015) and Motamed Dashliborun et al. (2016). The emulation tests were implemented on a hexapod ship motion simulator to mimic floating vessel motions whereas a capacitance Wire-Mesh Sensor (WMS) was used to measure the local instantaneous liquid saturation variations in the bed cross-section. Submitting the column to ship translational (surge, sway, heave) and rotational oscillations (roll, pitch, yaw, roll + pitch) worsened phase distribution and liquid axial dispersion in comparison with the conventional vertical beds. In addition, a shift in the regime transition from tickle flow to pulse flow towards higher fluid velocities was detected by increasing the oscillation periods of roll or roll + pitch motions. On the other hand, Iliuta and Larachi (2016a, b, c) recently developed a series of 3-D two-fluid transient models for simulation of gas-liquid downflow in vertical, slanted, and oscillating packed bed reactors. The numerical results revealed that angular oscillations of the packed bed prompted periodic variations of cross-sectionally averaged liquid holdups and two-phase pressure drop contrary to the stationary vertical and inclined configurations. They attributed this oscillatory behavior to the complex reverse secondary flows in the radial and circumferential directions. A delay in liquid drainage Iliuta and Larachi (2016c) and reduction of hydrodesulfurization performance Iliuta and Larachi (2016a) were also reported for the gas-liquid cocurrent downflow packed bed reactors as a result of oscillating motions.

As far as the open literature is concerned, the effect of ship translational and rotational oscillations on hydrodynamics of gas-liquid cocurrent upflow packed beds has not been yet addressed. Therefore, this contribution aims to provide important insights into the hydrodynamic features of cocurrent upflow packed bed reactors on floating platforms. The hydrodynamic

characteristics in terms of bed pressure drop, phase distribution, liquid saturation, and pulse flow regime are experimentally examined. Moreover, the residence time distribution (RTD) experiments are carried out to estimate the liquid residence time and the Péclet number in oscillating cocurrent upflow packed beds. To mimic FPSO movements, a hexapod ship motion simulator being able to impose a variety of motion scenarios including translations (heave, surge, and sway), rotations (roll, pitch, and yaw), and combinations thereof to an embarked packed bed is employed. Capacitance Wire-Mesh Sensors (WMSs) coupled with the packed bed is used to scrutinize on-line and locally the two-phase flow dynamic features as well as to detect the tracer pulses. Finally, the hydrodynamic behavior of cocurrent upflow packed beds under motion conditions is also compared with the bed limiting postures of stationary vertical and inclined configurations.

2. Experimental setup

2.1. Upflow packed bed components and hexapod platform

Laboratory-scale hydrodynamic experiments were carried out using air and water operated in the cocurrent upflow mode at room temperature and atmospheric pressure in a transparent 57 mm ID Plexiglas column packed with 3 mm glass beads up to a height of 1500 mm. The experimental setup is schematically shown in Fig. 1 together with the wire-mesh sensor (WMS) (3) applied for liquid saturation measurements and tracer pulse detection as well as the ship motion simulator (hexapod) (6). The fluid properties, the range of operating conditions and the packed bed specifications are summarized in Table 1. The packing was tightly clamped between a lowermost gas-liquid distributor (5) and uppermost mesh screen to avoid bed fluidization and to ensure synchronous movement with the reactor. The setup was operated in a recycle mode for the liquid phase, which was supplied and controlled by a peristaltic pump. The gas was separated from the

liquid at the top of the vessel by means of a gas-liquid separator (1) and then vented to the atmosphere. A multipoint gas-liquid distributor (5) was employed, which consisted of 22 needle orifices with 0.4 mm inner diameter for the gas supply and 9 capillaries with 1 mm inner diameter for the liquid feed. Pressure drops through the bed were measured using a differential pressure transmitter connected to the packed-bed reactor. The readings of this sensor were recorded over time and transferred to a standard PC running a LabVIEW program for the data acquisition.

As depicted in Fig. 1, the packed bed was firmly installed on a NOTUS hexapod platform (6) with six-degree-of-freedom motions including translations (surge, along Y direction; sway, along X direction; heave, along Z direction) and rotations (roll around Y axis; pitch around X axis; yaw around Z axis) to emulate actual floating vessel conditions. In addition to these single-degree-of-freedom motions, combined roll + pitch motions with 90° phase-lag were also tested in the present work. Each hexapod translational and rotational excitation was programmed by generating an effective sinusoidal motion path given by: $p = A_p sin(2\pi ft+\phi)$ with A_p is the amplitude (mm for translation or degree for rotation); f is the frequency (Hz); t is the effective duration of movements (period) and ϕ is the phase lag. The programmed parameters of the hexapod motion, which were compatible with conditions of a floating vessel under sea excitations (Abraham et al., 2015; Journée and Massie, 2000; Moskowitz, 1964), are summarized in Table 2. More detailed information about the hexapod ship motion emulator and representative video clips of the five types of column movements can be found in our previous works (Assima et al., 2015b; Motamed Dashliborun and Larachi, 2015). For the sake of comparison, stationary vertical (0°) and stationary inclined (5°, 10°, and 15°) packed bed configurations were also included in this study.

2.2. Wire-mesh sensor/ tracer tests

The capacitance wire-mesh sensor (WMS) with a matrix-like arrangement of the sensing points, providing high spatiotemporal images from the interrogated bed cross-section, was used for the liquid saturation measurements and detection of the tracer pulses. The aptitude of the sensor for the investigation of several multiphase flow phenomena has been proven for (i) gas-liquid flow in pipes (Prasser et al., 1998; Szalinski et al., 2010), (ii) multiphase flow in packed beds (Llamas et al., 2010; Schubert et al., 2010b) and open-cell foams (Mohammed et al., 2013), and recently (iii) for the hydrodynamic characterization of moving packed beds (Assima et al., 2015b; Motamed Dashliborun and Larachi, 2015; Motamed Dashliborun et al., 2016) as well as oscillating bubble columns (Assima et al., 2015a). This measuring technique gives access to images of liquid volumetric distributions in the entire bed cross-sections using as a contrasting property the difference between gas and liquid electrical permittivity values nearby the WMS sensing point voxels.

The WMS employed in this work consisted of two axially separated parallel planes, 1.5 mm afar, each made of 16 stainless steel wires with 3.57 mm lateral spacing. The wires in one plane were aligned perpendicularly to the wires in the other plane. This arrangement resulted in a theoretical number of 256 sensing points with 188 effective points inscribed inside the column circular cross-section. During the packing procedure, special care was taken to minimize the interference of the low-intrusive WMS with the packed bed by carefully filling the glass spheres into the voids of the wire mesh. As far as visual observations before, during and after column operation were concerned, the glass beads, especially those retained in the wire-mesh sensor portion did not exhibit any noticeable displacement with respect to their initial state. All liquid saturation results presented in the current study were obtained at a height of 400 mm before upper bed exit

with a framerate of 100 Hz. More detailed information about the WMS principle, functionality and calculation procedure can be found elsewhere (Da Silva et al., 2007; Da Silva, 2008; Llamas et al., 2007; Schubert et al., 2010b).

Two wire-mesh sensors flange-mounted at positions 400 mm (WMS 2) and 1240 mm (WMS 1) downstream the top of the packing were used to measure the temporal evolution of tracer pulses and the alteration of their shapes due to liquid back-mixing in the liquid flow along the bed. An aqueous sodium chloride solution (c_{NaCl} = 300 mg/L) was used as conductivity tracer and briefly injected for 5 s within the water stream. The conductivity of the liquid after tracer injection was monitored in the liquid storage tank by a conductivity meter. To prevent signal baseline drifts, accumulation of the tracer was avoided by regular replacement of the liquid with fresh deionized water.

If a conducting liquid is present at a sensing point of the sensor, the unknown complex impedance can be described as a dielectric consisting a capacitor (coupled to the permittivity of the fluid) and a resistor (coupled to the conductivity) (Da Silva, 2008). At an elevated conductivity, set to approximately 0.02 S/m in this work and depending on the preliminary calibration and setting procedure of the WMS electronics, the resistive part of the complex impedance becomes dominant and the measured signal is logarithmically dependent on the conductivity only (Da Silva, 2008). This characteristic is described by the calibration function given by Eq. 1, which links the measured voltage V per sensing point (i,j) to the conductivity K of the liquid or the corresponding tracer concentration, respectively:

$$V(i,j) = a_1(i,j) \times \log\left\{K^2(i,j) + a_2{}^2(i,j)\right\} + a_3(i,j) \qquad (1)$$

Where the constants $a_1(i,j)$, $a_2(i,j)$ and $a_3(i,j)$ depend on the geometry as well as on the electrical circuit of every sensing point and were estimated during the calibration of the WMS prior to the actual residence time distribution (RTD) measurements. The instantaneous pixel signals of the sensors were averaged in the cross-section and normalized to the total amount of tracer.

3. Results and discussion

3.1. Pressure drop

In packed beds with gas-liquid cocurrent upflow, the overall pressure drop consists of gas-liquid-solid interactions (i.e., dynamic pressure) and static head of the liquid phase. The hexapod motions and accelerations/decelerations are transmitted to the flowing fluids inside the porous medium and are expected to alter the hydrodynamics prevailing in the packed bed resulting in peculiar pressure drop fluctuations. Hence, the transient variation of the pressure drop was recorded in the moving packed bed after the column was exposed to various hexapod oscillations as described in Table 2. Such fluctuations can be straightforwardly captured observing the pressure drop time series in Fig. 2 for the roll (a) and roll + pitch (b) motions with a constant amplitude of ±15° evolving within periods of 5, 10 or 20 s, respectively. Pressure drops measured under identical flow rate conditions for the stationary vertical and the stationary 15°-inclined beds are also plotted for comparison.

In the rolling packed bed (Fig. 2a), the bed overall pressure drop evolved from minimum towards maximum with tilting the column from Θ = +15° to Θ = 0°within one-quarter motion period, reflecting a progressive growth from lowest to highest interactions. Conversely, the following sequence for the next quarter motion period, where the bed was tilted from Θ = 0° to Θ = -15°, led to the opposite trend in the pressure drop evolution. It is worth mentioning that the extent of

interphase interactions is an important function of the motion period. From Fig. 2a, it can be seen that decreasing the roll period from T = 20 s to T = 5 s results in attenuating the oscillation amplitudes at the expense of increasing pressure drops. The incidence of more recurring packed-bed acceleration/ deceleration triggered inertial disturbances contributing to the increase of pressure drop, whereas the oscillation amplitudes were shrunk by filtering effects of the high-frequency components. Contrary to the rolling column with an oscillation period of 5 s, where the bed overall pressure drop was higher than that of the stationary vertical bed for almost the entire period, there was a tendency for the pressure drops to slide below their vertical bed analogs by increasing the roll period. Still, at the approach of verticality of the moving column the pressure drop peaks kept noticeably higher than those corresponding to the stationary vertical bed reflecting the important contribution of inertial forces gained by the fluids in response to the column accelerations. On the other hand, the ±15° minima of the oscillating pressure drops were clearly below the stationary 15°-inclined bed pressure drop (dotted line, Fig. 2a). Such reduction can be ascribed to the presence of more bubbles, which, persisting in the cross-section of the rolling bed owing to the escalating transverse forces, reduced the contribution of static liquid head in the bed overall pressure drop. Likewise, the superimposed roll + pitch motion revealed nearly periodic oscillations in the pressure drop time series (Fig. 2b). Nevertheless, the periodicity of pressure oscillations was equivalent to the motion period and the oscillation amplitudes were markedly attenuated mainly due to restricting the gas-liquid flow by the alternating takeover of roll and pitch.

Unlike the observations made earlier, Fig. 2c show that oscillations became barely discernible in the pressure drop time series, when subjecting the packed bed to translational periodic motions, i.e., sway/surge (vertical column moving forward and backward, TY or TX) and heave (vertical

column sliding up and down, TZ), indicating that the two-phase flow remained virtually almost indifferent to such types of oscillatory perturbations. At the same imposed oscillation period, the yaw motion (vertical column wobbling around its revolution axis, RZ), on the contrary, augmented interphase interactions and brought about recognizable oscillations in the time series of bed overall pressure drop (red line, Fig. 2c). In general, both translational motions, whether normal or parallel to the fluid streams in the porous medium, as well as wobbling the vertical bed dramatically shifted the average bed overall pressure drop above the one prevailing for the stationary vertical packed bed (Fig. 2c).

3.2. Gas-liquid distribution

A uniformity factor, χ, was defined as a criterion to quantitatively assess the quality of liquid distribution based on the lack of crosswise uniformity of the liquid saturation over the bed cross-section, when it is subjected to different hexapod motion scenarii (Patel et al., 2008):

$$\chi = \frac{1}{NP}\sum_{i=1}^{NP}\left(\frac{\beta_i - \overline{\beta}}{\overline{\beta}}\right)^2 \tag{2}$$

where NP is the number of pixels in the image obtained from the wire-mesh sensor, β_i and β are the corresponding i^{th} pixel liquid saturation and the cross-sectionally averaged liquid saturation, respectively. Here, increasing values of the uniformity factor indicate worsening of the homogeneous distribution of the liquid in the interrogated bed cross-section.

Fig. 3 illustrates the time-series variations of the uniformity factor prompted by different hexapod tilting and non-tilting movements already mentioned for the corresponding pressure drop time-series. In all cases, the gas and liquid superficial velocities were kept constant. While instantaneous values of the uniformity factor objectified periodic behavior for the roll and roll +

pitch motions or the so-called tilting motions (Figs. 3a,b), such oscillations went more or less undetected for non-tilting motions, i.e, yaw, heave, and surge, (Fig. 3c) similarly to their corresponding pressure drop time-series (Fig. 2c). Nevertheless, these tilting motions degraded the quality of gas-liquid distribution as compared with the stationary vertical configuration.

Column angular movements in the course of hexapod roll and roll + pitch excitations caused time-dependent gravitational and inertial (acceleration/deceleration) forces prompting secondary transverse displacements of the fluids in the bed crosswise planes. Consequently, transverse flow in the radial and circumferential directions induced those notable amplitude oscillations in the uniformity factor time series as is evident from Figs. 3a,b. It should be noticed that under roll motion, the uniformity factor reached its maximum value by tilting the bed to $\Theta = \pm 15°$ whereas changing the position from $\Theta = \pm 15°$ to $\Theta = 0°$ led to the minimum value in the uniformity factor time series (Fig. 3a), which is exactly the opposing behavior compared to the pressure drop signal. These maxima and minima reached by the uniformity factor were found to depend strongly on the rolling period as also observed for the pressure drop. Interestingly, the uniformity factor during the rolling motions at higher period durations exhibited overshoots with respect to the stationary 15°-inclined bed. This corroborated the existence of more bubbles in the cross-section of the rolling bed resulting in higher phase maldistribution as compared with the stationary 15°-inclined bed. Therefore, reliance on the stationary inclined columns, corresponding to the maximum angular amplitude, as a representative of the maximum uniformity factor is proven to be unreliable. Besides, as the roll motion quietened, the oscillation amplitudes increased and the homogeneity of the liquid distribution continued to worsen. This rests on the fact that more defined flow patterns temporarily evolved in the gentler rolling packed beds. The same cannot be concluded from the uniformity factor time series of the oscillations

excited by the roll + pitch motion since the amplitudes decreased noticeably by the alternating takeover of roll and pitch where the gas and liquid phases gradually interchanged their positions along the lower wall of the bed often off-vertical posture (Fig. 3b).

The WMS measurements confirmed the fact that the roll and roll + pitch motions significantly influence the gas-liquid flow hydrodynamics inside the packed bed. To further highlight the gas-liquid displacement during the column angular oscillations, iso-surface visualizations in the form of 3-D Eulerian representations of the gas-liquid instantaneous patterns in the packed bed subjected to different motion periods of the roll and the roll + pitch are illustrated in Figs. 4b,c, respectively. For direct comparison, the gas-rich and liquid-rich presence for the stationary vertical and the 15°-inclined beds are presented in Fig. 4a in a similar fashion.

As seen from Fig. 4a, the relatively even distribution of gas and liquid in the stationary vertical packed bed was deteriorated while tilting the bed by 15° forcing gas bubbles to migrate towards the upper wall region and accumulating liquid in the lower wall region, thus developing permanent phase segregation zones. However, the column rolling incited a transverse zigzag motion in the gas-liquid flow patterns (Fig. 4b) clearly deviating from the nearly vertical and inclined trajectories observed, respectively, in the stationary vertical and 15°-inclined configurations (Fig. 4a). Similarly, the alternative takeover of roll and pitch motions due to 90° phase lag aroused those irregularities in the gas-liquid flow patterns in the porous medium (Fig. 4c). While the roll + pitch motion positioned the column in such a manner to be permanently tilted at 15°, its rotation around the central vertical axis imposed a swirling pattern in the gas-liquid flow. Such spatial discrepancy in the gas-liquid distribution of the entire bed length led to the rich variability of the bed overall pressure signals as shown in Figs. 2a,b. It is worthy of notice that the wall-to-wall liquid and bubble migrations remained matching with the motion

period for both tilting motions. These 3-D visualizations helped to ascertain a supplementary effect of gravity when combined with inertia on the complexity of the packed-bed hydrodynamics under tilting motions.

3.3. Residence time distribution and liquid dispersion

Liquid dispersion in the packed bed additionally affected by column tilts and oscillations was also investigated. The axial dispersion plug flow model (ADM) with open-open boundary conditions was used to estimate the liquid residence time and the effective Péclet number (Delgado, 2006; Levenspiel, 1999). Signals from the WMS were fitted to the two-parameter ADM by employing the imperfect-pulse Aris method with non-linear fitting in the time-domain (Wakao and Kagei, 1982). The calculated mean liquid residence time and effective Péclet number are presented and discussed with respect to the gas-liquid flow patterns shown above.

Fig. 5 shows the effect of bed inclination on the mean liquid residence time and liquid effective Péclet number. To recognize the dispersive phenomena, the tracer signals registered by the lower and upper wire mesh sensors are plotted in Fig. 5a. Excellent agreement was found between measured and back-calculated output signals for all column tilt angles (results not shown here). As can be seen from Fig. 5b, slightly tilting the bed by 5° resulted in a noticeable decrease of the mean liquid residence time because of facilitation of the passage of the major part of the tracer at the lower wall region, whereas it increased persistently with further tilting the bed on account of evolving gas-liquid disengagement zones objectified before (Fig. 4a, 15°-inclined bed). Though tracer migration was relatively fast in the lower liquid-rich region, the slower liquid flow in the upper gas-rich region tended to spread part of the tracer leading to an increase in liquid residence time. In addition, the column inclination was found to appreciably influence the effective Péclet number. Fig. 5b illustrates a monotonic decline in the effective Péclet number as a result of bed

tilt due to the emerging segregated flow pattern, where the liquid flow became more dispersive. This is evident from the widened tracer signals of the inclined packed beds in comparison with those corresponding to the vertical bed (Fig. 5a).

The contribution to liquid dispersion by the hexapod tilting excitations in the packed bed was studied next. The tracer responses for the bed subjected to different periods of roll and roll + pitch motions are shown in Figs. 6a,b, respectively. Under identical flow rate conditions, the solid and dashed black lines illustrated in Fig. 6 show tracer responses, respectively, for the stationary vertical and 15° inclined bed configurations in order to make a direct comparison. Obviously, the transverse zigzag (roll) and swirl (roll + pitch) motions of liquid flow resulted in more axial dispersion as exposed from widened tracer signals and lower Péclet numbers in comparison with the corresponding stationary vertical bed (Fig. 6a,b). Moreover, an increasing motion period translated into a reduction of the Péclet number and an increase in liquid residence time for both tilting motions. These observations highlighted the fact that the temporary development of gas-liquid segregated flow patterns in the packed bed under the high oscillation period (20 s) led to more severe liquid back-mixing. Yet, the effective Péclet number and the mean liquid residence time for the oscillating packed beds were away from those corresponding to the stationary 15° inclined bed since the time needed to complete the tracer elution was much longer in such inclined posture without any movement.

In addition, the tracer responses of the packed bed with non-tilting motions (yaw, heave, and yaw) are shown in Fig. 7a jointly with the back-calculated signals. Unlike in the packed bed with tilting oscillations, the effective Péclet number remained almost comparable with the value of the stationary vertical bed indicating less departure from liquid plug flow character, though the mean liquid residence time was noticeably decreased by the column vertical standing movements (Fig.

7b). Among the tested non-tilting motions, heave manifested the lowest Péclet numbers and the highest mean liquid residence time, which can be imputed to the extra liquid back-mixing provoked by the vertical sliding up and down of the packed bed. Interestingly, the tracer signal modes and shapes for all column tilt angles and motion scenarii (tilting and non-tilting) remained practically consistent with those corresponding to the stationary vertical bed.

3.4. Pulse flow regime

In addition to the hydrodynamic characteristics under prevailing bubbly flow or segregated/bubbly flow, the effect of packed bed oscillation and motion period on the pulse flow regime was also examined. Representative time-series of the cross-sectionally averaged liquid saturation are shown for roll (Fig. 8b) and roll + pitch (8c) motions following two motion periods of 5 s and 20 s as well as for the stationary vertical and 15° inclined beds (Fig. 8a). In all cases, gas and liquid superficial velocities were constant. To highlight the evolving flow structure, 3-D Euler representations of gas-rich and liquid-rich presence and liquid pulse are also presented in Fig. 9 in correspondence with Fig. 8 modalities. As seen from both figure sets, a clear pulsing flow became visible in the stationary vertical whereas those widespread pulses tended to disappear with inclining the bed by 15° as a consequence of the formation of the segregated/bubbly flow regime (Figs. 8a,9a). As highlighted earlier, the gravity-driven force in the 15°-inclined bed diminished the gas-liquid interaction by preferentially pulling liquid to the lower wall region and facilitating gas bubbles to escape toward the upper wall region.

Examination of the pulsing flow regime after the bed was subjected to the roll motion revealed that pulse inception and amplitude were strictly controlled by the oscillation period (Figs. 8b,9b). The rolling period of 20 s manifested an intermittent pulsing flow regime, the emergence of which coincided with straightening of the column posture during oscillations, i.e., from Θ = +15°

(or -15°) to Θ = 0°. By approaching to verticality, the gas-rich and liquid-rich regions tended to gradually disappear yielding intensified gas-liquid interactions and emergence of pulses thereof. Nevertheless, rolling the bed by 5 s periods did not exhibit such liquid pulses. This was attributed to the increase in the breakup rate of gas/liquid slugs by virtue of the intensified transverse forces in the bed cross-section stemming from the relatively fast angular oscillation of the column. In the roll + pitch motion, on the other hand, liquid pulses covering almost the entire bed cross-section were not observed for both the 5 s and 20 s motion periods as illustrated in Figs. 8c,9c. This observation highlights the fact that an off-vertical position due to the 90° phase lag between roll and pitch prevented accumulation of more liquid in the bed voidage, thus dramatically diminishing competition between gas and liquid to occupy the pores.

The above results revealed that the flow regime prevailing in the oscillating packed bed was quite different from the one occurring in the stationary vertical and the 15° inclined bed configurations. To highlight this difference, two orthogonal regions adjacent to the wall were selected from the 2-D WMS slice, as illustrated in Fig. 10 with red (region RI) and blue (region RII) colors inside a circle representing the bed cross-section. The instantaneous evolutions of the spatially-averaged liquid saturation for these regions were plotted in Figs. 10a,b, respectively, for roll and roll + pitch motions.

A noticeable spatial inhomogeneity in the crosswise liquid distribution is evident from the zonal liquid saturation time series for roll and roll + pitch motions. While the liquid saturation of RI exhibited a periodic behavior by rolling the bed due to being subjected frequently to the lowermost position (Θ = +15°) and the uppermost position (Θ = -15°), RII was found to be almost unaffected in response to the column rolling though it was also adjacent to the wall (Figs. 10a1,a2). Conversely, the roll + pitch motion induced significant oscillations in the liquid

saturation time series of both RI and RII. Oscillations observed in Figs. 3a,b for the uniformity factor can be attributed to these periodic behaviors of regions in the bed cross-section.

In addition, further examination of the zonal liquid saturation for roll and roll + pitch motions revealed the coexistence of different flow regimes in the moving packed bed. The dispersed bubbly flow regime was reflected as high-frequency low-amplitude fluctuations in the crests, whereas the smoothed character of liquid saturation time series along with its lower values in the troughs suggested existence of a spray-like flow regime, where liquid phase became dispersed in the form of droplets and gas phase became the continuous phase (Figs. 10a1,b1-2). For the rolling bed, relatively high-amplitude fluctuations reminiscent of intermittent liquid pulses can be pinpointed at the approach of the crests, where the column reached to the vertical position (Fig. 10a). Those pulses, however, were found to be barely discriminated in the liquid saturation time series of RII (Fig. 10a2).

The effect of an increase of liquid superficial velocity (U_g = 0.005 m/s) on the prevalence of pulsing flow in the zonal regions described above was also examined for roll and roll + pitch motions under 5 s and 20 s oscillating periods. For the sake of conciseness, here only the results of the liquid saturation time series for RI are presented (Fig. 11). Corresponding instantaneous variation of cross-sectionally averaged liquid saturations are also shown inside each graph on the top-right corner. As seen from Fig. 11, augmented liquid superficial velocity appreciably intensified the gas-liquid interactions leading to the formation of more pulses for both roll and roll + pitch motions (Figs. 11a,b). Interestingly, pulses emerged both in troughs and crests, regardless of the motion period, by increasing liquid superficial velocity. This was interpreted as due to the attainment of fully developed pulses being able to temporarily disperse the liquid over

the entire cross-section of the oscillating bed despite persistence of a periodic behavior in the liquid saturation.

4. Conclusion

The effect of ship oscillations and tilt on the hydrodynamic behavior of packed beds with cocurrent gas-liquid upflow mode of operation was experimentally studied. A column packed with 3 mm glass beads was positioned firmly on a hexapod ship motion simulator being able to emulate single and compound degrees of freedom, i.e., translations (heave, surge, and sway) and rotations (roll, pitch, and yaw). Wire-mesh sensors (WMSs) were embedded in the packed bed to register the local instantaneous liquid saturation variations across the bed in order to characterize their flow patterns in the course of the bed excitations. Furthermore, residence time distribution experiments were conducted to determine liquid mean residence time and Péclet number using tracer signal analysis and Aris's two-point detection method. The experimental findings indicated that:

- All column oscillations induced a noticeable impact on the bed overall pressure drops and gas-liquid distribution. While roll and roll + pitch or the so-called tilting motions brought about remarkable oscillations in the pressure drop and uniformity factor time series, the non-tilting motions (i.e., surge, heave, and yaw) was found to augment these parameters though with some minor fluctuations.
- Increasing tilt angle of the stationary bed led to decreasing the Péclet number and augmenting the liquid mean residence time due to the development of gas-liquid disengagement zones.

- The transverse zigzag (roll) and swirl (roll + pitch) motions of liquid flow resulted in more axial dispersion, whereas the Péclet number in the packed bed with the non-tilting motions remained almost comparable with the value of the stationary vertical bed.
- The tilting oscillations dramatically mitigated gas-liquid interactions by virtue of temporarily gravity-driven segregated flow patterns inside the bed resulting in a delay in the inception of pulsing flow regime.
- The rolling period of 20 s manifested an intermittent pulsing flow regime, the emergence of which coincided with straightening of the column posture during oscillations.
- Augmented liquid superficial velocity appreciably intensified the gas-liquid interactions leading to the formation of more pulses for both roll and roll + pitch motions.

Acknowledgments

The authors gratefully acknowledge the Natural Sciences and Engineering Research Council of Canada and the Canada Research Chair on Sustainable Energy Processes and Materials for their financial support.

Nomenclature

a	constant
A_p	Amplitude (degree/mm)
c	concentration (mol/L)
D	dispersion coefficient (m^2/s)
f	frequency (Hz)
H	axial distance from the top of packing
i,j	pixel index

K	conductivity (S/m)
L	axial distance between the wire-mesh sensors (m)
n	column rotational velocity (rpm)
N	time-series length
NP	number of pixels in bed cross-section (-)
Pe	Péclet number ($u_L L/\varepsilon_L D_{ax}$)
r	radial position (m)
R	reactor radius (m)
t	time (s)
T	period (s)
U	superficial velocity (m/s)
V	voltage (V)

Greek Letters

θ	angular position during roll or roll + pitch motion (°)
β	spatial-averaged liquid saturation
$\bar{\beta}$	time-averaged liquid saturation
ϕ	phase lag
χ	degree of uniformity (-)
τ	residence time (s)

Subscripts

ax		axial
	g	gas
	l	liquid

Abbreviations

ADM	axial dispersion model
RTD	residence time distribution
WMS	wire-mesh sensor
2-D	two-dimensional
3-D	three-dimensional

References

Abraham, E., Engineer, P.S.M., Olean, N., Miller, H., 2015. Meeting Base Package Design Requirements for Service on Floating Production, Storage and Offloading Vessels. 2015. http://www.dresser-rand.com/wp-content/uploads/2015/02/engineers_notebook winter2015.pdf

Assima, G.P., Larachi, F., Schleicher, E., Schubert, M., 2015a. Capacitance wire mesh imaging of bubbly flows for offshore treatment applications. Flow measurement and instrumentation 45, 298-307.

Assima, G.P., Motamed-Dashliborun, A., Larachi, F., 2015b. Emulation of gas-liquid flow in packed beds for offshore floating applications using a swell simulation hexapod. AIChE journal 61, 2354-2367.

Wongkia, A., Larachi, F., Assabumrungrat, S., 2015. Hydrodynamics of countercurrent gas-liquid flow in inclined packed beds–A prospect for stretching flooding capacity with small packings. Chemical Engineering Science 138, 256-265.

Atta, A., Schubert, M., Nigam, K., Roy, S., Larachi, F., 2010. Co-current descending two-phase flows in inclined packed beds: Experiments versus simulations. The Canadian Journal of Chemical Engineering 88, 742-750.

Attou, A., Ferschneider, G., 1999. A simple model for pressure drop and liquid hold-up in packed-bed bubble reactors. Chemical Engineering Science 54, 5139-5144.

Bouteldja, H., Hamidipour, M., Larachi, F., 2013. Hydrodynamics of an inclined gas–liquid cocurrent upflow packed bed. Chemical Engineering Science 102, 397-404.

Collins, J.H., Sederman, A.J., Gladden, L.F., Afeworki, M., Kushnerick, J.D., Thomann, H., 2016. Characterising gas behaviour during gas–liquid co-current up-flow in packed beds using magnetic resonance imaging. Chemical Engineering Science, http://dx.doi.org/10.1016/j.ces.2016.04.004i.

Da Silva, M., Schleicher, E., Hampel, U., 2007. Capacitance wire-mesh sensor for fast measurement of phase fraction distributions. Measurement Science and Technology 18(7), 2245.

Da Silva, M.J., 2008. Impedance sensors for fast multiphase flow measurement and imaging.

Motamed Dashliborun, A., Larachi, F., 2015. Hydrodynamics of gas–liquid cocurrent downflow in floating packed beds. Chemical Engineering Science 137, 665-676.

Motamed Dashliborun, A., Larachi, F., Hamidipour, M., 2016. Cyclic operation strategies in inclined and moving packed beds—Potential marine applications for floating systems. AIChE journal. DOI: 10.1002/aic.15327

Delgado, J., 2006. A critical review of dispersion in packed beds. Heat and mass transfer 42, 279-310.

Duduković, M.P., Larachi, F., Mills, P.L., 2002. Multiphase catalytic reactors: a perspective on current knowledge and future trends. Catalysis reviews 44, 123-246.

El-Reedy, M.A., 2012. Offshore structures: design, construction and maintenance. Gulf Professional Publishing, Oxford, United Kingdom.

Gu, Y., Ju, Y., 2008. LNG-FPSO: Offshore LNG solution. Frontiers of Energy and Power Engineering in China 2, 249-255.

Hofmann, H., 1983. Cocurrent upflow in fixed beds. In: Cheremisinoff, N.P., Gupta, R. (Eds.), Handbook of Fluids in Motion. Ann Arbor Science Publishers, Ann Arbor, MI, ISBN-13: 978-0250404582.

Iliuta, I., Larachi, F., 2016a. Hydrocarbon hydrodesulfurization in vertical, inclined and oscillating trickle beds–Hydrodynamics & reactor performance for offshore petroleum marine applications. Fuel 186, 35-49.

Iliuta, I., Larachi, F., 2016b. Three-dimensional simulations of gas-liquid cocurrent downflow in vertical, inclined and oscillating packed beds. AIChE journal 62, 916-927.

Iliuta, I., Larachi, F., 2016c. Two-fluid simulation of liquid drainage in oscillating packed beds for offshore floating applications. Chemical Engineering Science 149, 51-62.

Jo, D., Revankar, S.T., 2011. Investigation of bubble breakup and coalescence in a packed-bed reactor–Part 1: A comparative study of bubble breakup and coalescence models. International Journal of Multiphase Flow 37, 995-1002.

Journée, J., Massie, W., 2000. Offshore hydromechanics. Delft University of Technology, Delft (the Netherlands): Available from: http://www.shipmotions.nl/DUT/LectureNotes.

Khadilkar, M., Wu, Y., Al-Dahhan, M., Duduković, M., Colakyan, M., 1996. Comparison of trickle-bed and upflow reactor performance at high pressure: model predictions and experimental observations. Chemical Engineering Science 51, 2139-2148.

Kim, H.-J., Choi, D.-K., Ahn, S.-I., Kwon, H., Lim, H.-W., 2014a. GTL FPSO—An Alternative Solution to Offshore Stranded Gas. Paper presented at: Offshore Technology Conference, Houston, Texas, USA.

Kim, W.S., Yang, D.R., Moon, D.J., Ahn, B.S., 2014b. The process design and simulation for the methanol production on the FPSO (floating production, storage and off-loading) system. Chemical Engineering Research and Design 92, 931-940.

Larachi, F., Laurent, A., Wild, G., Midoux, N., 1991. Some experimental liquid saturation results in fixed-bed reactors operated under elevated pressure in cocurrent upflow and downflow of the gas and the liquid. Industrial & Engineering Chemistry Research 30, 2404-2410.

Levenspiel, O., 1999. Chemical reaction engineering. 3rd ed. New York: Wiley, 1999.

Leveque, J., Philippe, R., Zanota, M.-L., Meille, V., Sarrazin, F., Baussaron, L., de Bellefon, C., 2016. Hydrodynamics and mass transfer in a tubular reactor containing foam packings for intensification of GLS catalytic reactions in co-current up-flow configuration. Chemical Engineering Research and Design 109, 686-697.

Llamas, J.-D., Lesage, F., Wild, G., 2007. Local liquid saturation measurements inside a trickle bed reactor operating near the transition between pulsing and trickling flow. Chemical Engineering Science 62, 7225-7232.

Llamas, J.-D., Lesage, F., Wild, G., 2010. Radial dispersion in trickle-bed reactors: Comparison between sock and dense loadings. Chemical Engineering Science 65, 538-541.

Mohammed, I., Bauer, T., Schubert, M., Lange, R., 2013. Hydrodynamic multiplicity in a tubular reactor with solid foam packings. Chemical Engineering Journal 231, 334-344.

Moreira, M.F., Freire, J.T., 2003. Influence of gas and liquid flow rates and the size and shape of particles on the regime flow maps obtained in concurrent gas-liquid downflow and upflow through packed beds. Industrial & Engineering Chemistry Research 42, 929-936.

Moskowitz, L., 1964. Estimates of the power spectrums for fully developed seas for wind speeds of 20 to 40 knots. Journal of geophysical research 69, 5161-5179.

Murugesan, T., Sivakumar, V., 2002. Pressure drop and flow regimes in cocurrent gas–liquid upflow through packed beds. Chemical Engineering Journal 88, 233-243.

Patel, A.K., Waje, S.S., Thorat, B.N., Mujumdar, A.S., 2008. Tomographic diagnosis of gas maldistribution in gas–solid fluidized beds. Powder technology 185, 239-250.

Prasser, H.-M., Böttger, A., Zschau, J., 1998. A new electrode-mesh tomograph for gas–liquid flows. Flow measurement and instrumentation 9, 111-119.

Raghavendra Rao, A.V., Kishore Kumar, R., Sankarshana, T., Khan, A., 2011. Identification of Flow Regimes in a Concurrent Gas Liquid Upflow through Packed Beds. Chemical Engineering & Technology 34, 1909-1917.

Ranade, V.V., Chaudhari, R., Gunjal, P.R., 2011. Trickle bed reactors: reactor engineering & applications. Elsevier.

Salgi, P., Balakotaiah, V., 2014. Impact of gravity on the bubble-to-pulse transition in packed beds. AIChE journal 60, 778-793.

Schubert, M., Hamidipour, M., Duchesne, C., Larachi, F., 2010a. Hydrodynamics of cocurrent two-phase flows in slanted porous media—Modulation of pulse flow via bed obliquity. AIChE journal 56, 3189-3205.

Schubert, M., Khetan, A., Da Silva, M.J., Kryk, H., 2010b. Spatially resolved inline measurement of liquid velocity in trickle bed reactors. Chemical Engineering Journal 158, 623-632.

Shimamura, Y., 2002. FPSO/FSO: State of the art. Journal of marine science and technology 7, 59-70.

Subrata, K., Cliakrabarti, S., 2005. Handbook of offshore engineering. Vol I: Amsterdam: Elsevier Ocean Engineering Series.

Szalinski, L., Abdulkareem, L., Da Silva, M., Thiele, S., Beyer, M., Lucas, D., Perez, V.H., Hampel, U., Azzopardi, B., 2010. Comparative study of gas–oil and gas–water two-phase flow in a vertical pipe. Chemical Engineering Science 65, 3836-3848.

Varma, Y., Khan, A., Khan, A., 1997. Flow regime identification and pressure drop in cocurrent gas-liquid upflow through packed beds. Bioprocess Engineering 16, 355-360.

Vejražka, J., Večeř, M., Orvalho, S., Sechet, P., Ruzicka, M.C., Cartellier, A., 2010. Measurement accuracy of a mono-fiber optical probe in a bubbly flow. International Journal of Multiphase Flow 36, 533-548.

Wakao, N., Kagei, S., 1982. Heat and mass transfer in packed beds. Gordon and Breach Science Publishers: New York.

Table Captions

Table 1 Ranges of operating conditions and system properties.

Table 2 Hexapod kinematic parameters during packed column motion.

Table 1.

Parameter	**Value/Range**
Gas superficial velocity, U_g	0.0016-0.10 m/s
Liquid superficial velocity, U_l	0.0025-0.005 m/s
Liquid phase density, ρ_L	998 kg/m^3
Liquid viscosity, μ_L	0.001 Pa s
Liquid surface tension, σ_L	0.072 N/m
Gas density, ρ_g	
Spherical glass beads size, d_p	0.003 m
Bed porosity, ε	0.395
Bed length, L	1.5 m
Reactor diameter, ID	0.057 m

Table 2.

Motion	**Oscillation period (s)**	**Phase (°)**	**Amplitude (mm or °)**
Roll (RY)	5.0/ 10.0/ 20.0	0	θ [-15 – +15°]
Roll + Pitch (RY + RX)	5.0/ 20.0	90° for RX & 0° for RY	[-15 – +15°] & [-15 – +15°]
Yaw (RZ)	5.0	0	[-15 – +15°]
Heave (TZ)	5.0	0	[-200 – +200] mm
Sway (TY)	5.0	0	[-250 – +250] mm

Figure Captions

Figure 1 Schematic diagram of the experimental setup for the stationary-oscillating packed bed with gas-liquid cocurrent upflow mode together with wire-mesh sensor and hexapod emulated elementary translational and rotational motions.

Figure 2 Effect of different motions on the overall bed pressure drop at U_g = 0.016 m/s and U_l = 0.0025 m/s: (a) roll, (b) roll + pitch, (c) non-tilting oscillations (surge/sway, heave, and yaw). Pressure drop for stationary vertical and 15° inclined columns under similar flow rate conditions are drawn for comparison.

Figure 3 Effect of packed bed oscillation on the uniformity factor, χ: (a) roll, (b) roll + pitch, (c) non-tilting oscillations (surge/sway, heave, and yaw) at U_g = 0.016 m/s and U_l = 0.0025 m/s. Time series of the uniformity factor for stationary vertical and 15° inclined columns under similar flow rate conditions are drawn for comparison.

Figure 4 3-D iso-surface visualization of gas-rich and liquid-rich presence for packed beds with (a) stationary vertical and 15° inclined postures, (b) roll motion, and (c) roll + pitch motion at U_g = 0.016 m/s and U_l = 0.0025 m/s.

Figure 5 (a) Measured inlet and outlet WMS response curves in the stationary packed bed with different inclination angles and (b) mean liquid residence time and liquid effective axial Péclet number as a function of bed inclination (U_g = 0.016 m/s and U_l = 0.0025 m/s).

Figure 6 Measured inlet and outlet WMS response curves in oscillating packed beds with different periods under (a1) roll motion and (b1) roll + pitch motion;

corresponding mean liquid residence time and liquid effective axial Péclet number for (a2) roll motion and (b2) roll + pitch motion at U_g = 0.016 m/s and U_l = 0.0025 m/s. Corresponding results for stationary vertical and 15° inclined beds under similar flow rate conditions are drawn for comparison.

Figure 7 (a) Measured inlet and outlet WMS response curves together with the fit of the outlet response to the ADM in stationary vertical beds and under non-tilting motions and (b) corresponding mean liquid residence time and liquid effective axial Péclet number at U_g = 0.016 m/s and U_l = 0.0025 m/s.

Figure 8 Instantaneous cross-sectional averaged liquid saturation for packed beds with (a) stationary postures, (b) roll motion, and (c) roll + pitch motion at U_g = 0.10 m/s and U_l = 0.0025 m/s.

Figure 9 3-D iso-surface visualization of gas-rich and liquid-rich presence and liquid pulse for packed beds with (a) stationary postures, (b) roll motion, and (c) roll + pitch motion at U_g = 0.10 m/s and U_l = 0.0025 m/s.

Figure 10 Liquid saturation time series in two different wall regions (RI and RII) of same bed cross-section for the packed bed under (a) roll motion and (b) roll + pitch motion for 20 s oscillating period (U_g = 0.10 m/s and U_l = 0.0025 m/s).

Figure 11 Effect of liquid superficial velocity on pulsing dominance in region RI of the packed bed under (a) roll motion and (b) roll + pitch motion with different oscillating periods (U_g = 0.10 m/s and U_l = 0.005 m/s). Corresponding time series of cross-sectional averaged liquid saturation is also drawn on top-right corner of each graph.

Figure 1

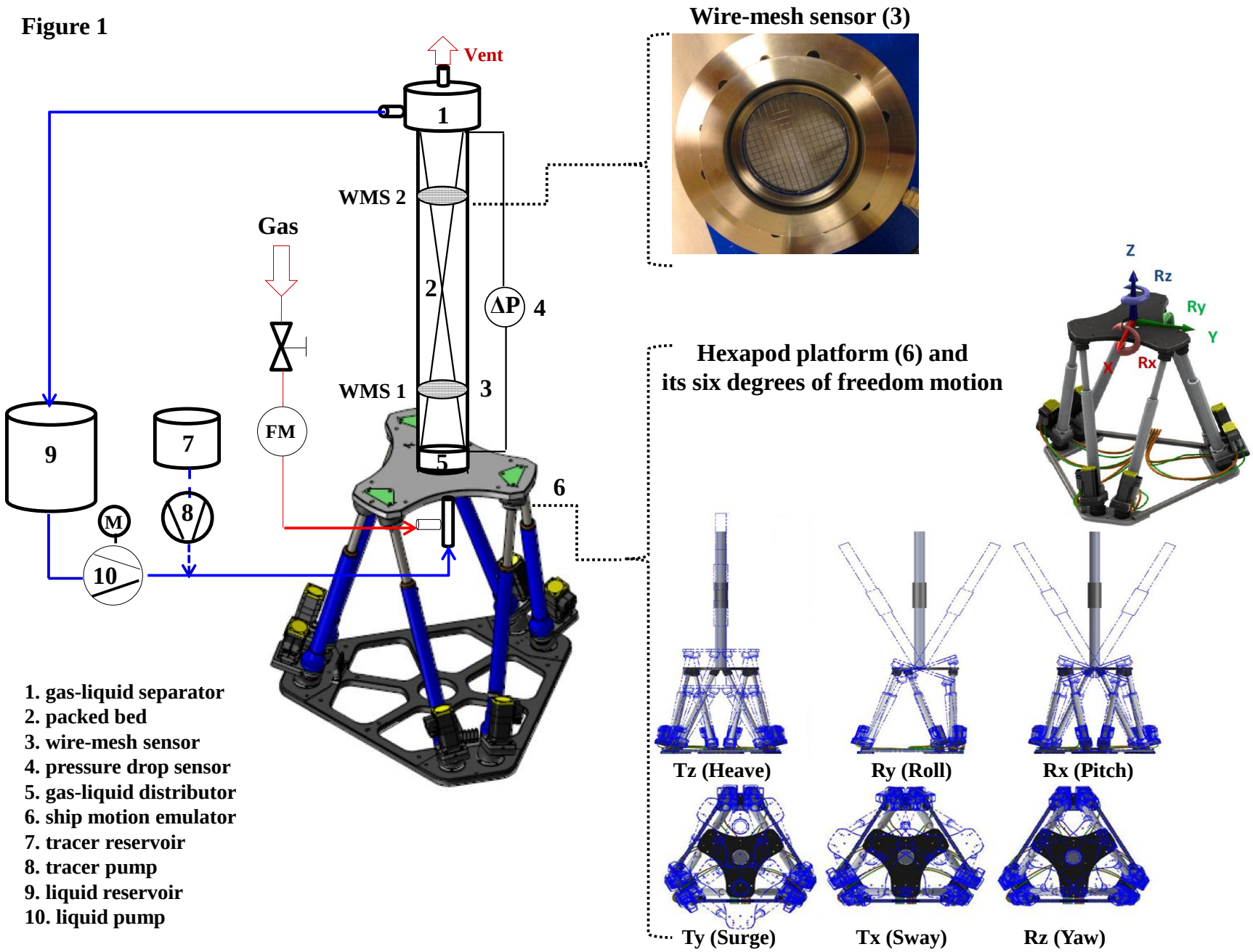

1. gas-liquid separator
2. packed bed
3. wire-mesh sensor
4. pressure drop sensor
5. gas-liquid distributor
6. ship motion emulator
7. tracer reservoir
8. tracer pump
9. liquid reservoir
10. liquid pump

Figure 2

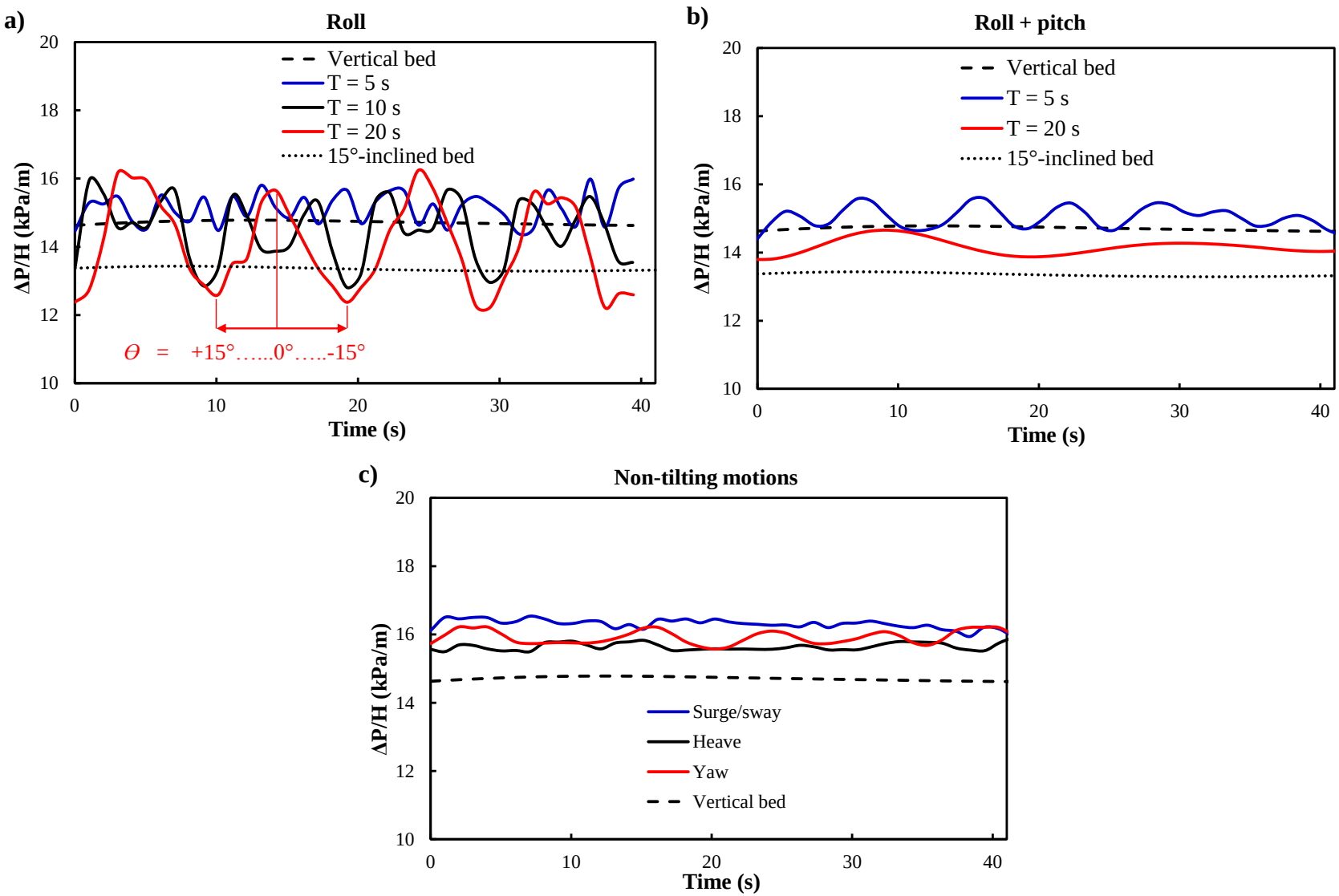
a)
Roll
Vertical bed
T = 5 s
T = 10 s
T = 20 s
15°-inclined bed
ΔP/H (kPa/m)
Θ = +15°…...0°…..-15°
Time (s)
b)
Roll + pitch
Vertical bed
T = 5 s
T = 20 s
15°-inclined bed
ΔP/H (kPa/m)
Time (s)
c)
Non-tilting motions
Surge/sway
Heave
Yaw
Vertical bed
ΔP/H (kPa/m)
Time (s)

Figure 3

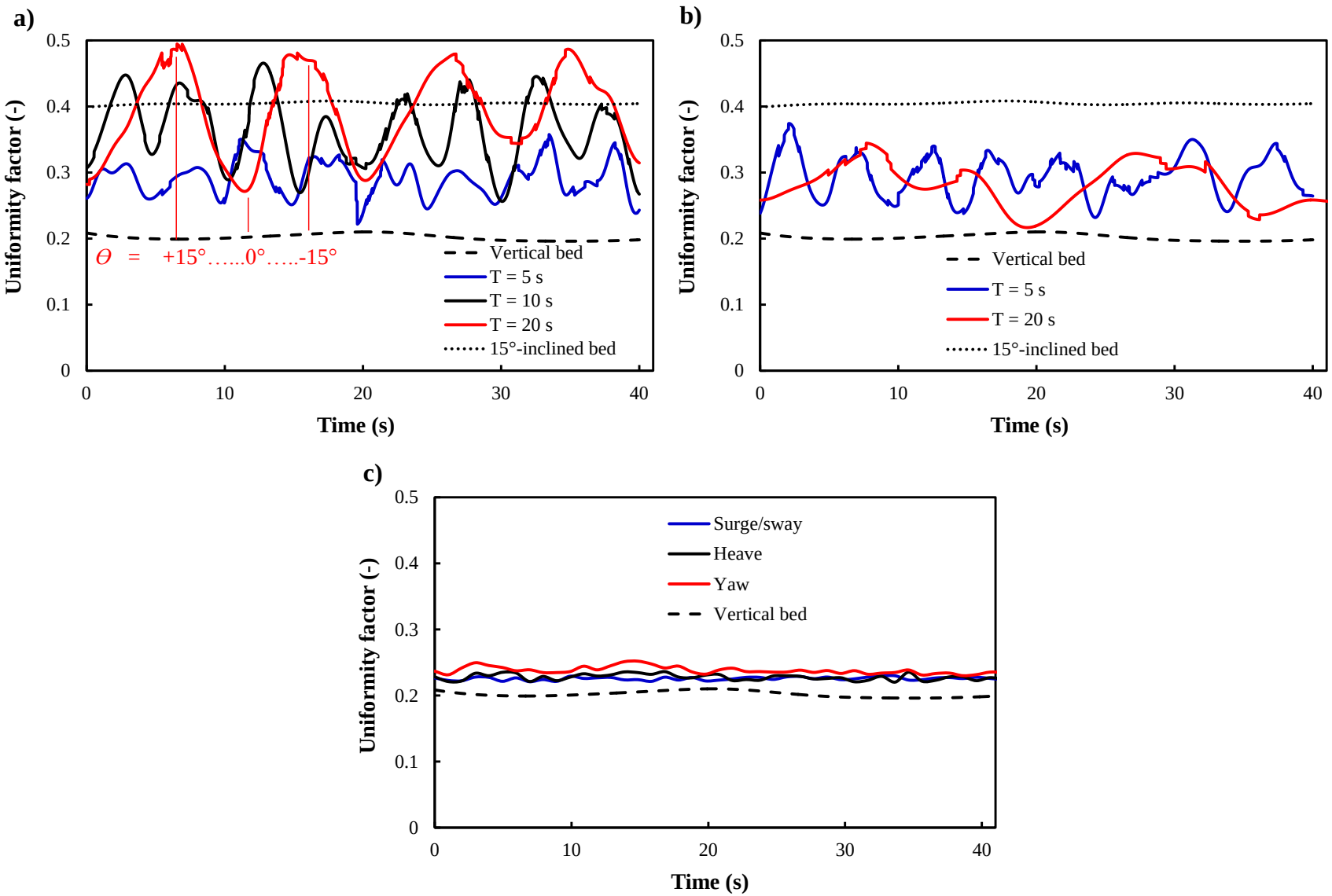
a)
Uniformity factor (-)
Time (s)
Θ = +15°……0°…..-15°
Vertical bed
T = 5 s
T = 10 s
T = 20 s
15°-inclined bed
b)
Uniformity factor (-)
Time (s)
Vertical bed
T = 5 s
T = 20 s
15°-inclined bed
c)
Uniformity factor (-)
Time (s)
Surge/sway
Heave
Yaw
Vertical bed

Figure 4

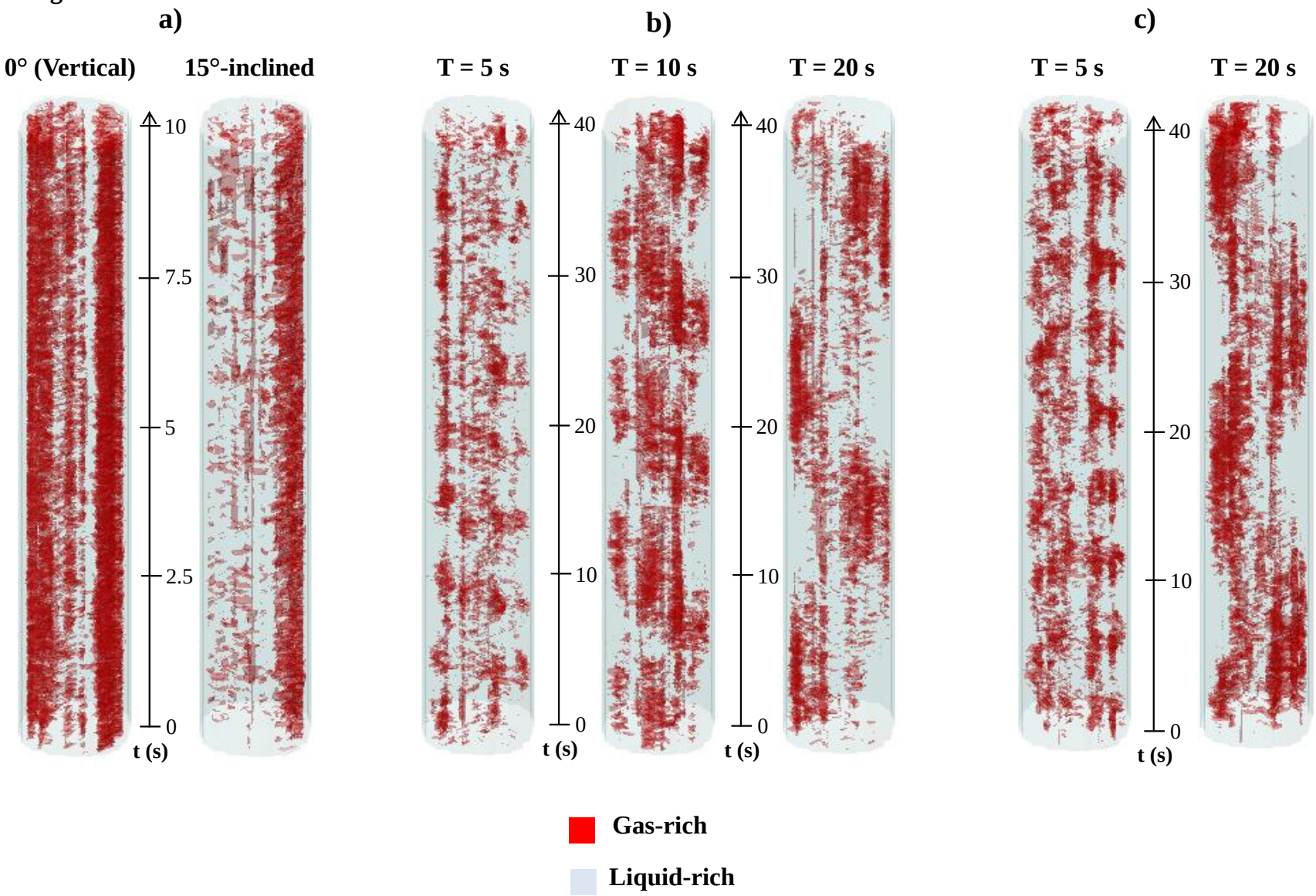
a)
0° (Vertical)
15°-inclined
10
7.5
5
2.5
0
t (s)
b)
T = 5 s
T = 10 s
T = 20 s
40
30
20
10
0
t (s)
c)
T = 5 s
T = 20 s
40
30
20
10
0
t (s)
Gas-rich
Liquid-rich

Figure 5

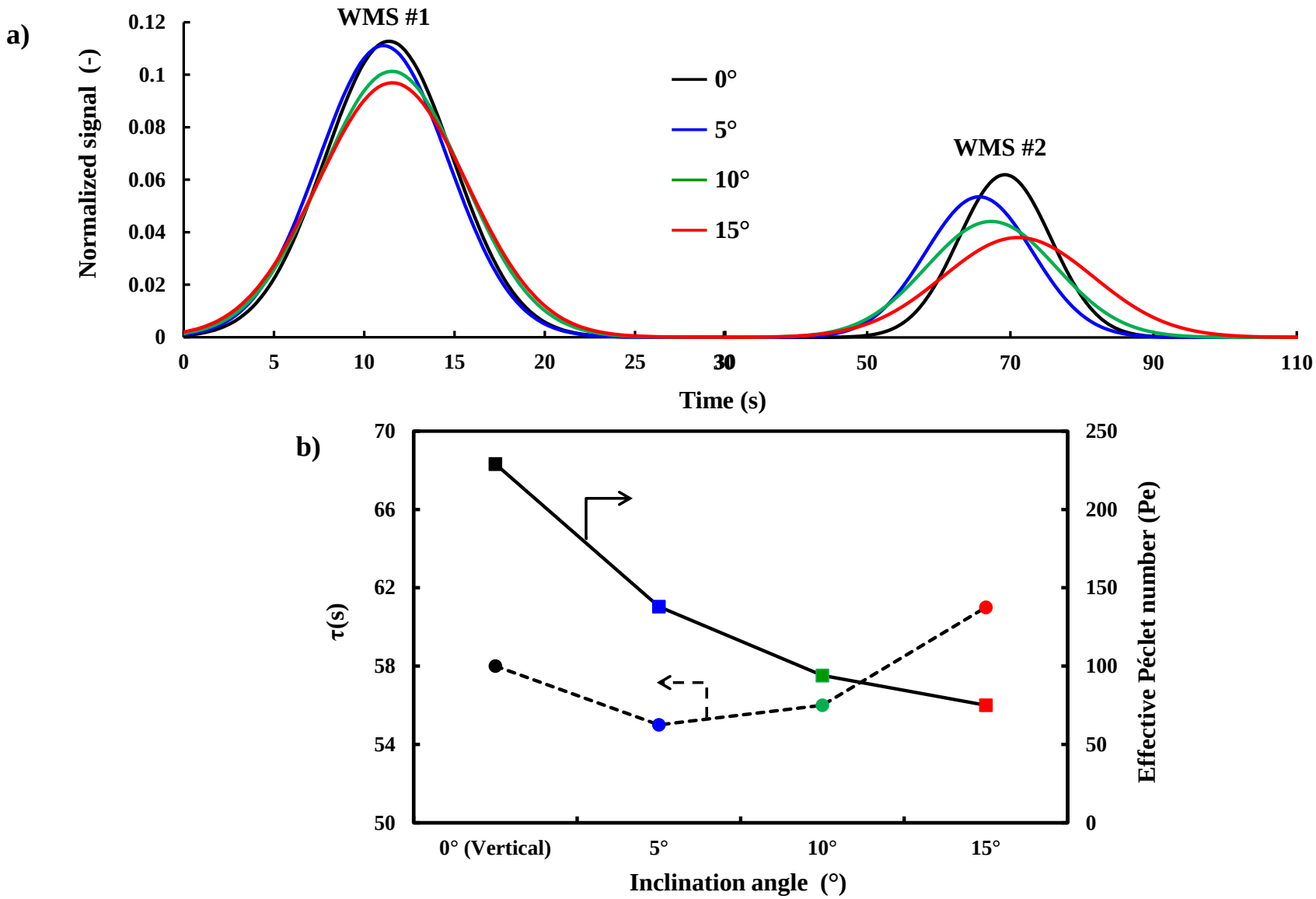
a)
WMS #1
WMS #2
0°
5°
10°
15°
Normalized signal (-)
Time (s)
0.12
0.1
0.08
0.06
0.04
0.02
0
0
5
10
15
20
25
30
50
70
90
110
b)
τ(s)
Effective Péclet number (Pe)
Inclination angle (°)
0° (Vertical)
5°
10°
15°
70
66
62
58
54
50
250
200
150
100
50
0

Figure 6

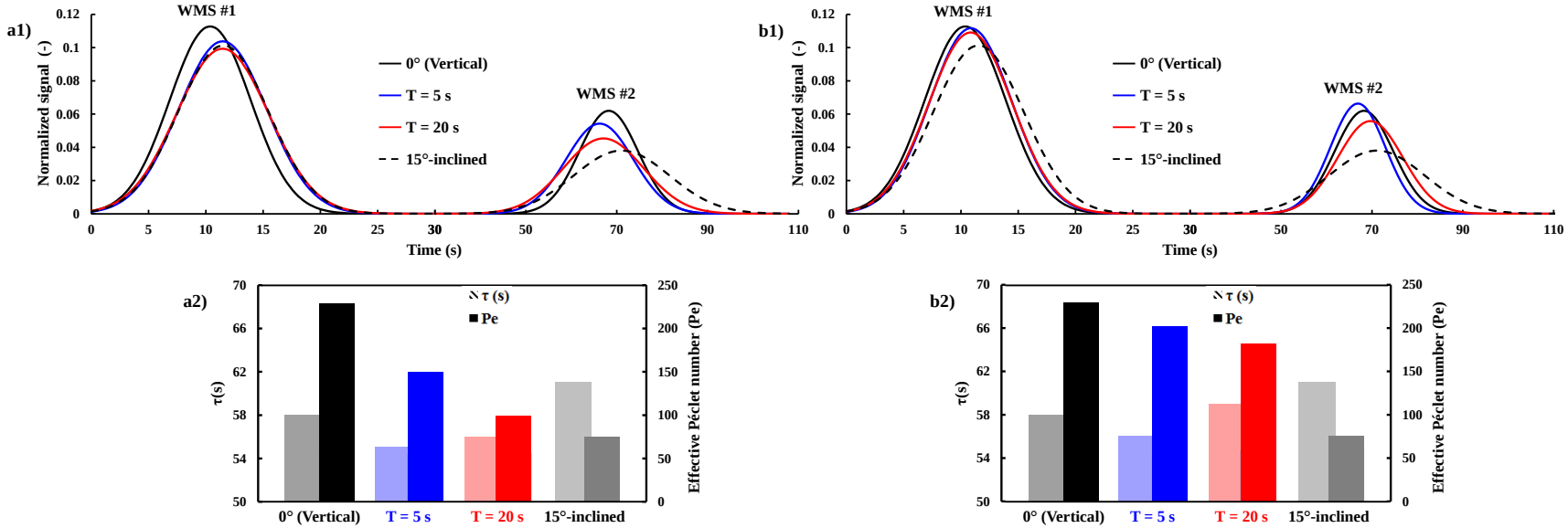
a1)
WMS #1
WMS #2
Normalized signal (-)
Time (s)
0° (Vertical)
T = 5 s
T = 20 s
15°-inclined
b1)
a2)
b2)
τ (s)
Pe
Effective Péclet number (Pe)
0° (Vertical)
T = 5 s
T = 20 s
15°-inclined

Figure 7

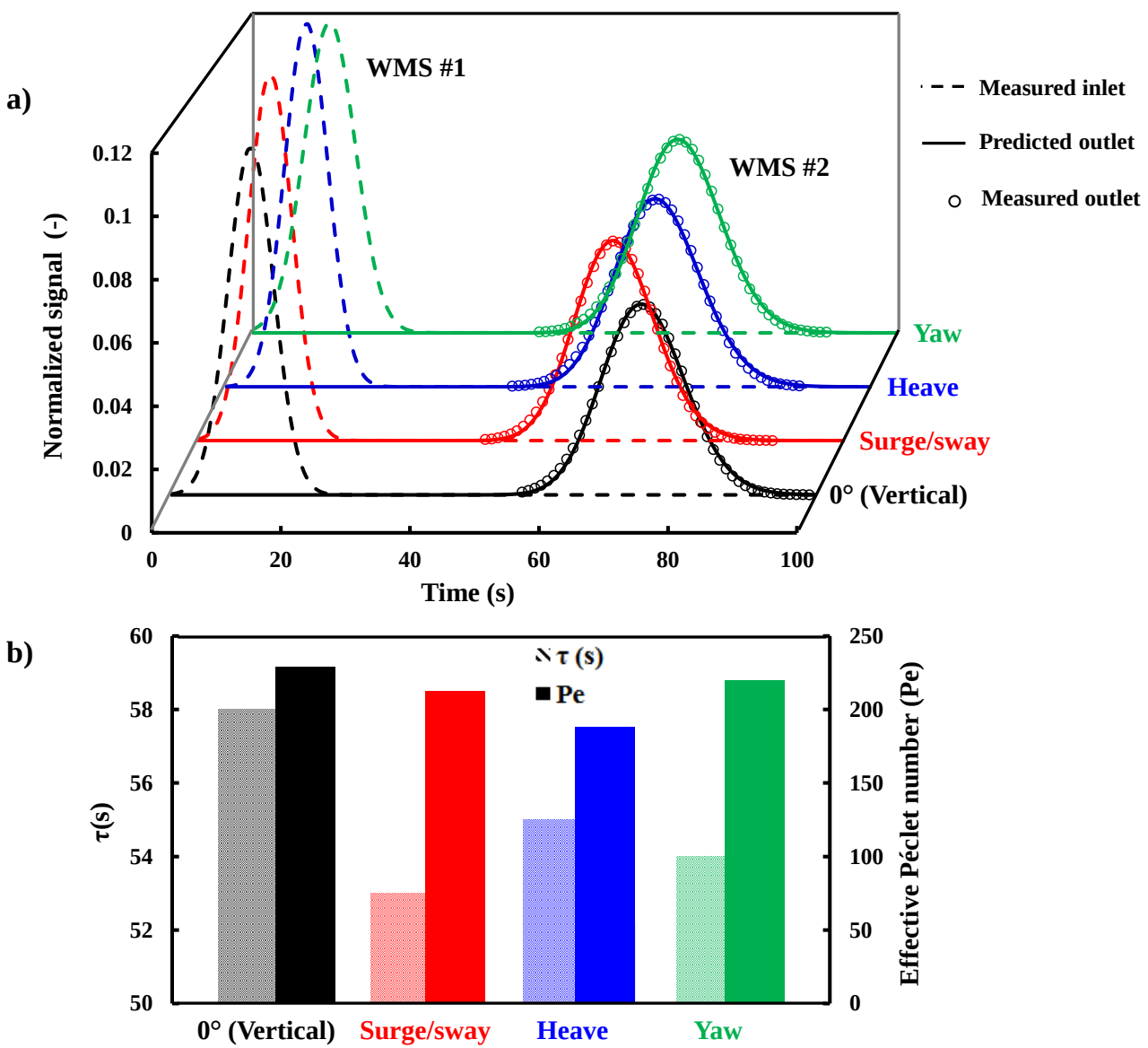
a)
WMS #1
WMS #2
Measured inlet
Predicted outlet
Measured outlet
Yaw
Heave
Surge/sway
0° (Vertical)
Normalized signal (-)
0.12
0.1
0.08
0.06
0.04
0.02
0
0
20
40
60
80
100
Time (s)
b)
τ (s)
Pe
τ(s)
60
58
56
54
52
50
250
200
150
100
50
0
Effective Péclet number (Pe)
0° (Vertical)
Surge/sway
Heave
Yaw

Figure 8

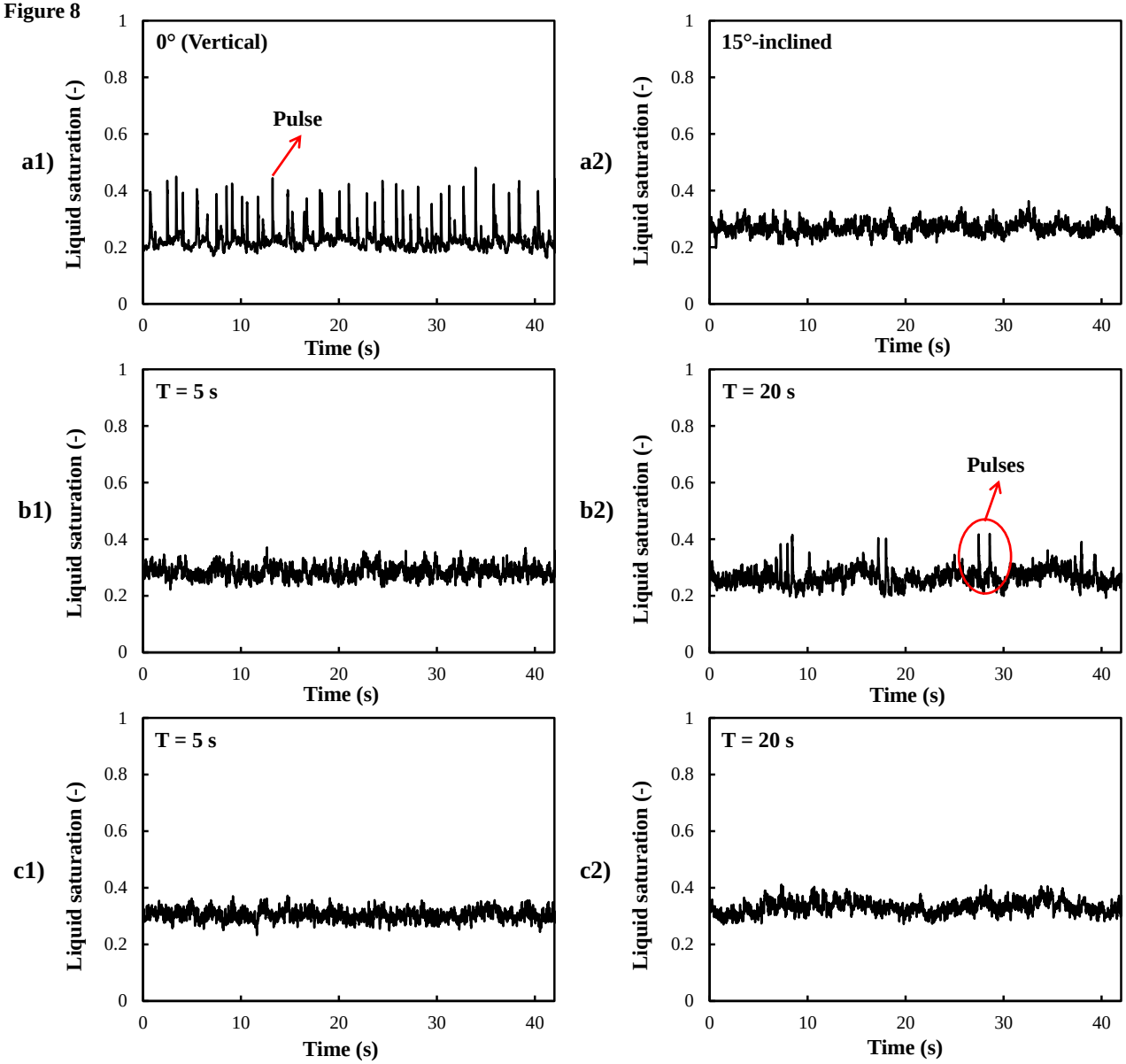
a1)
0° (Vertical)
Pulse
a2)
15°-inclined
b1)
T = 5 s
b2)
T = 20 s
Pulses
c1)
T = 5 s
c2)
T = 20 s
Liquid saturation (-)
Time (s)
0
0.2
0.4
0.6
0.8
1
0
10
20
30
40

Figure 9

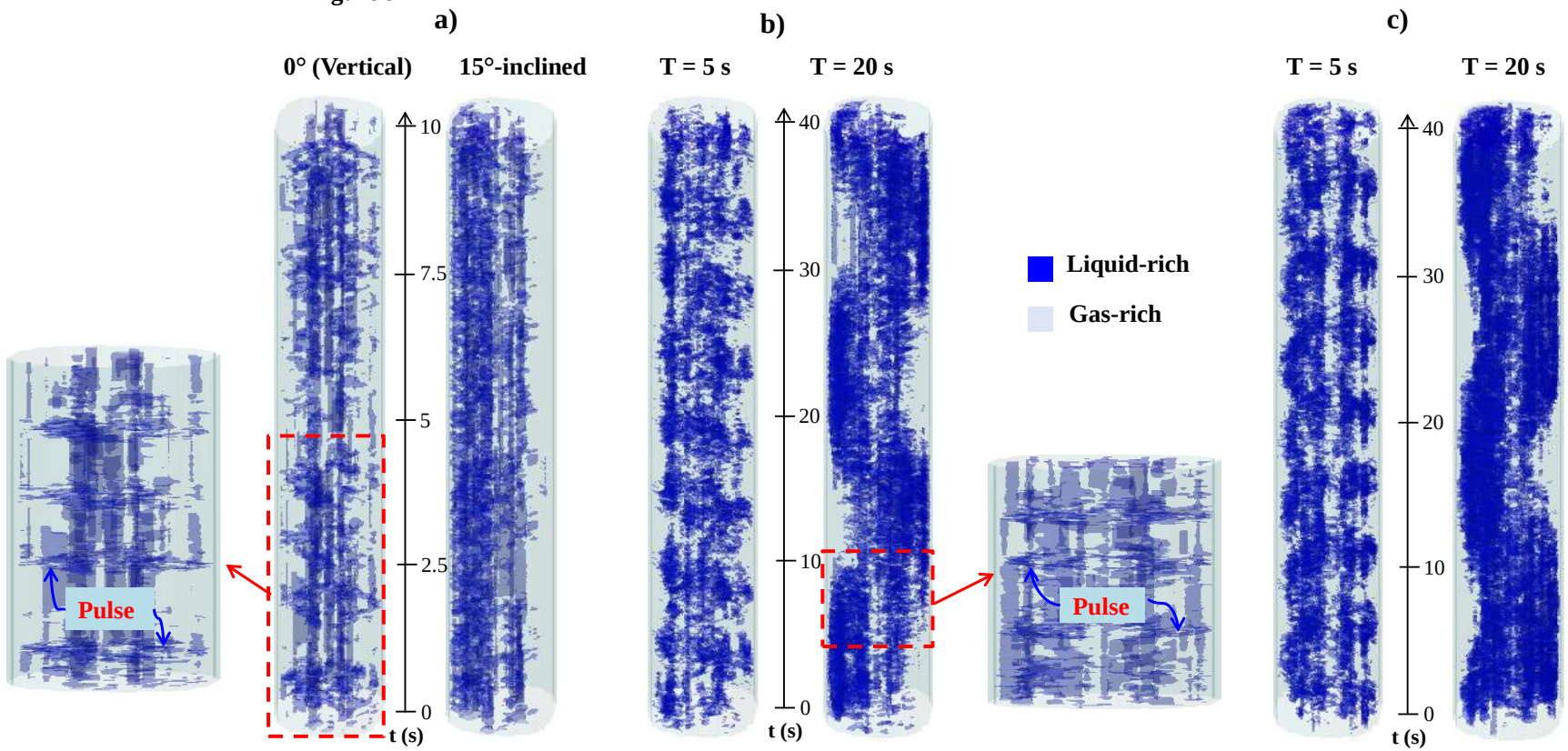
a)
0° (Vertical)
15°-inclined
10
7.5
5
2.5
0
t (s)
Pulse
b)
T = 5 s
T = 20 s
40
30
20
10
0
t (s)
Pulse
Liquid-rich
Gas-rich
c)
T = 5 s
T = 20 s
40
30
20
10
0
t (s)

Figure 10

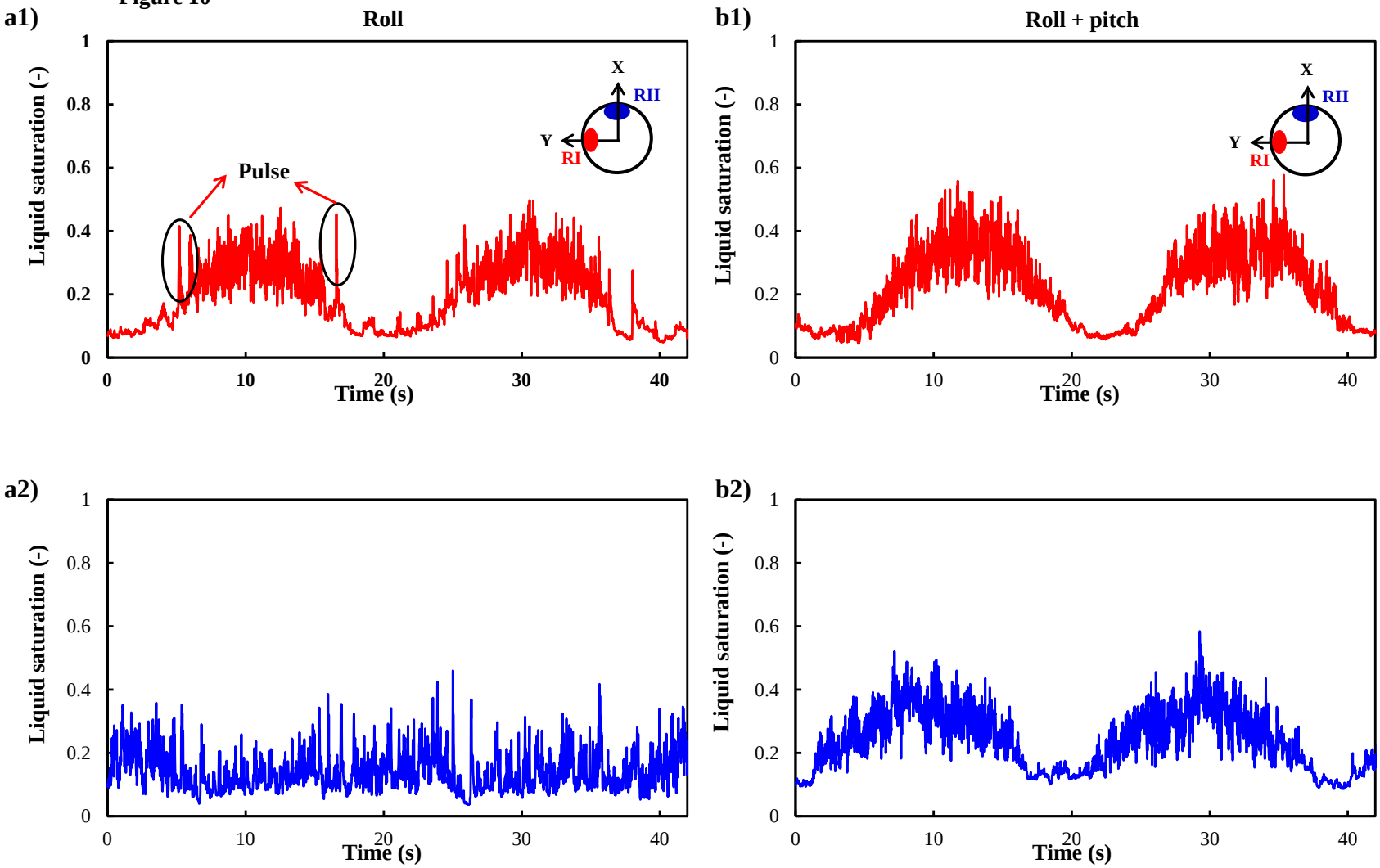
a1)
Roll
Liquid saturation (-)
Time (s)
Pulse
X
Y
RII
RI
b1)
Roll + pitch
Liquid saturation (-)
Time (s)
X
Y
RII
RI
a2)
Liquid saturation (-)
Time (s)
b2)
Liquid saturation (-)
Time (s)

Figure 11

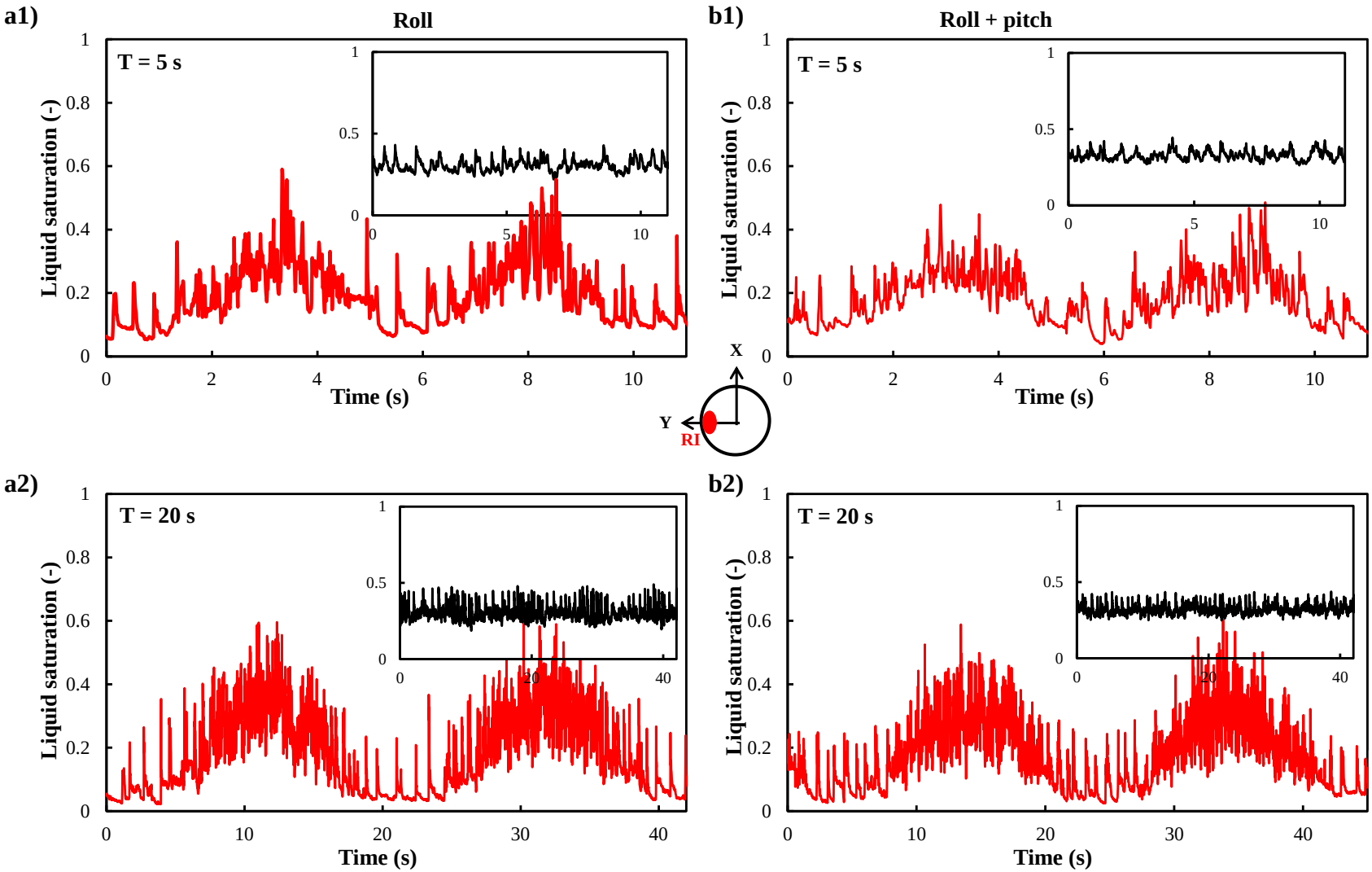
a1)
Roll
T = 5 s
Liquid saturation (-)
Time (s)
b1)
Roll + pitch
T = 5 s
Liquid saturation (-)
Time (s)
X
Y
RI
a2)
T = 20 s
Liquid saturation (-)
Time (s)
b2)
T = 20 s
Liquid saturation (-)
Time (s)